Reversible Bridge-Mediated Excited-State Symmetry Breaking in Stilbene-Linked DNA Dumbbells

ARTICLE *in* THE JOURNAL OF PHYSICAL CHEMISTRY B · APRIL 2008

Impact Factor: 3.3 · DOI: 10.1021/jp710718p · Source: PubMed

Reversible Bridge-Mediated Excited-State Symmetry Breaking in Stilbene-Linked DNA Dumbbells

Frederick D. Lewis,*,† Pierre Daublain,† Ligang Zhang,† Boiko Cohen,† Josh Vura-Weis,† Michael R. Wasielewski,*,† Vladimir Shafirovich,*,§ Qiang Wang,‡ Milen Raytchev,‡ and Torsten Fiebig*,‡

Department of Chemistry, Northwestern University, Evanston, Illinois 60208-3113, Department of Chemistry, Boston College, Chestnut Hill, Massachusetts 02467, and Department of Chemistry, New York University, New York, New York 10003

Received: November 8, 2007; In Final Form: December 20, 2007

The excited-state behavior of synthetic DNA dumbbells possessing stilbenedicarboxamide (Sa) linkers separated by short A-tracts or alternating A−T base-pair sequences has been investigated by means of fluorescence and transient absorption spectroscopy. Electronic excitation of the Sa chromophores results in conversion of a locally excited state to a charge-separated state in which one Sa is reduced and the other is oxidized. This symmetry-breaking process occurs exclusively via a multistep mechanism—hole injection followed by hole transport and hole trapping—even at short distances. Rate constants for charge separation are strongly distance-dependent at short distances but become less so at longer distances. Disruption of the A-tract by inversion of a single A−T base pair results in a pronounced decrease in both the rate constant and efficiency of charge separation. Hole trapping by Sa is highly reversible, resulting in rapid charge recombination that occurs via the reverse of the charge separation process: hole detrapping, hole transport, and charge return to regenerate the locally excited Sa singlet state. These results differ in several significant respects from those previously reported for guanine or stilbenediether as hole traps. Neither charge separation nor charge recombination occur via a single-step superexchange mechanism, and hole trapping is slower and detrapping faster when Sa serves as the electron donor. Both the occurrence of symmetry breaking and reversible hole trapping by a shallow trap in a DNA-based system are without precedent.

Introduction

Excited-state symmetry breaking occurs when the locally excited state of a symmetric bichromophoric molecule A*−A is converted to the charge-separated state $A^{+\bullet}-A^{-\bullet}$.[1] This process normally requires both high solvent polarity and strong through-bond coupling between chromophores, as is the case for 9,9′-bianthryl, the classic example of symmetry breaking.[2] Symmetry breaking has also been observed for conformationally mobile 1,2-dianthrylethanes[3] and for perylenediimide dimers and aggregates having cofacial geometries.[4] Bridge-mediated symmetry breaking in symmetric A−B−A systems has received relatively little attention. Adams and co-workers recently postulated that bridge-mediated symmetry breaking in perylenediimide dimers separated by 0 to 3 *p*-phenylene bridging units yields the $A^{+\bullet}-B-A^{-\bullet}$ charge-separated state via a single-step superexchange mechanism.[5,6]

We report here the results of our collaborative investigation of the excited-state behavior of the A−B−A type synthetic DNA dumbbells $Sa-A_n-Sa$ having stilbenediamide (Sa) chromophore linkers separated by 1 to 5 A−T base pairs (Chart 1). Weak exciton coupling (EC) between the Sa chromophores in dumbbells 1−5 which have poly(dA):poly(dT) sequences (A-tracts) was observed in the circular dichroism (CD) spectra of the dumbbell conjugates and of their capped hairpin analogs.[7,8] The sign and intensity of the EC-CD spectra is strongly dependent upon the dihedral angle as well as the distance between Sa chromophores. The initial objective of the present investigation was to determine whether the electronically excited Sa chromophores behave independently or if excitation is delocalized, as it is in cofacial stilbene dimers and stilbenophanes which display excimer fluorescence.[9] We find that the excitation is initially localized on a single Sa, but that the electronically excited dumbbells undergo symmetry breaking to yield $Sa^{-\bullet}-$

CHART 1: Structures of (a) Sa and Sd Chromophores and (b) Sa Conjugates

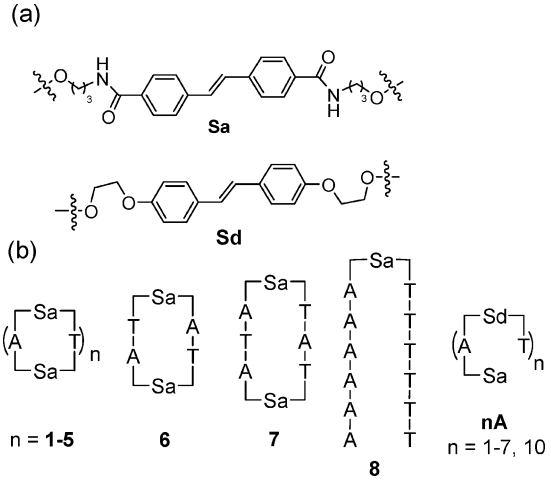

* Corresponding authors. E-mail: (Lewis) fdl@northwestern.edu; (Wasielewski) m-wasielewski@northwestern.edu; (Shafirovich) vs5@nyu.edu; (Fiebig) fiebig@bc.edu.
† Northwestern University.
‡ Boston College.
§ New York University.

10.1021/jp710718p CCC: $40.75
Published on Web 03/05/2008

SCHEME 1: Kinetic Scheme for Hole Injection, Hole Transport, and Charge Recombination in Dumbbell 4

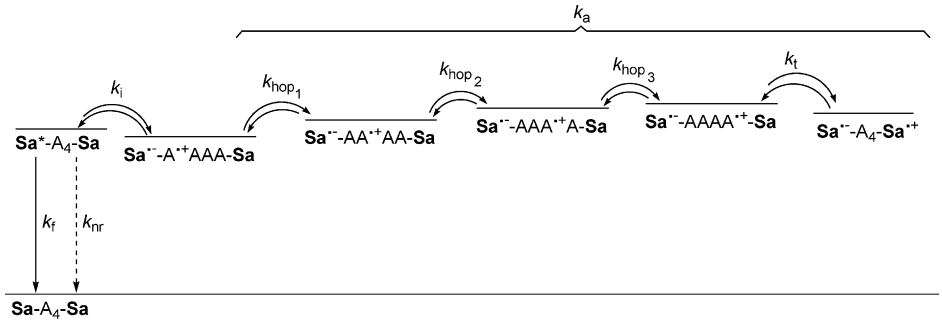

TABLE 1: Fluorescence Quantum Yields and Fluorescence Decay Data for Dumbbells 1−5 and Hairpin 8[a]

conjugate	Φ_f[b]	τ_1, ns[c,d]	τ_2, ns[c,e]	τ_3, ns[c,e]
1	0.32	0.094 (81)	1.2 (08)	5.2 (11)
2	0.33	0.17 (65)	1.1 (19)	4.3 (16)
3	0.34	0.24 (42)	1.7 (50)	5.4 (08)
4	0.30	0.087 (60)	1.6 (36)	4.7 (04)
5	0.33	0.12 (52)	1.8 (43)	3.7 (05)
8[f]	0.38	0.045 (71)	0.86 (08)	2.2 (21)

[a] Data obtained in aqueous solution (standard buffer). [b] Fluorescence quantum yields determined using 340 nm excitation by comparison of the peak areas with that obtained for a standard quinine sulfate solution in aqueous H_2SO_4 (0.5 M); estimated error: ±10%. [c] Fluorescence decay lifetimes (relative amplitudes in parentheses) for **1**−**5**, determined from triple exponential fits of the 390 nm decay obtained upon 350 nm excitation. [d] Component attributed to reversible hole injection to A_n. [e] Components attributed to charge return from $Sa^{-\bullet}-A_n^{+\bullet}-Sa$ and $Sa^{-\bullet}-A_n-Sa^{\bullet+}$. [f] Data from ref 11.

$A_n-Sa^{+\bullet}$ charge-separated states via a multistep mechanism consisting of photoinduced hole injection into the base-pair domain followed by hole transport and hole trapping (Scheme 1). The dynamics and efficiency of hole trapping are strongly dependent upon the distance between chromophores and upon the base-pair sequence, and they are indicative of rate-limiting hole transport when the chromophores are separated by several base pairs. Charge return through the A-tract bridges occurs via reversal of this process: thermal detrapping of the hole followed by hole transport and electron−hole recombination to yield locally excited $^1Sa^*$. Rate constants for detrapping are much faster than for guanine, which is a deeper hole trap than Sa. The occurrence of symmetry breaking and charge return via bridge-mediated hole hopping are without precedent in DNA or any other A−B−A system.

Results

Synthesis, Absorption, and Fluorescence. The syntheses of the Sa-linked dumbbells **1**−**5** have previously been reported, and their structures have been investigated using a combination of exciton-coupled circular dichroism spectroscopy and molecular modeling.[8] Dumbbells **6** and **7** were prepared from nicked dumbbell precursors using the chemical ligation procedure employed for **1**−**5**.[8] The UV absorption spectra of **1**−**7** (Figure S1)[10] are similar to that of hairpin **8** which possesses a single Sa chromophore. They have a long-wavelength band with a maximum at 335 nm assigned to the stilbene chromophore and a 260 nm band dominated by nucleobase absorption. A small blue-shift in the long-wavelength absorption maximum of **1** (330 nm) is attributed to weak exciton coupling.[7]

The fluorescence spectra of **1**−**5** resemble that of hairpin **8** and all have band maxima at 385 nm (Figure S2)[10] and similar fluorescence quantum yields (Table 1). Values of $\Phi_f = 0.32 \pm 0.02$ for **1**−**5** are independent of the length or sequence of the base-pair domain and are similar to the value for hairpin **8**. Fluorescence decays for **1**−**5** were determined using a Ti:sapphire-based laser system having a time resolution of about 35 ps.[11] Decay times and preexponentials obtained from triple exponential fits are reported in Table 1. As previously reported for hairpin **8** and for $Sa-A_n-Sd$ systems,[11] triple exponential fits provide one short-lived component (100−200 ps) and two longer-lived components (1−5 ns).

Pump−Probe Experiments. Femtosecond (fs) time-resolved transient absorption spectra for dumbbells **1**−**7** in aqueous solution were obtained using 350 nm excitation from either of two Ti:sapphire-based systems having a time resolution of about 100 fs. System 1 (used for dumbbells **1**−**3**) provides a spectral range of 350−750 nm and a time window of 0−1.8 ns,[11] and System 2 (used for dumbells **3**−**8**) provides a spectral range of 450−800 nm and a time window of 0−6 ns.[12] Transient spectra are shown in Figures 1 and 2 for **1** and **5**, respectively, and in Figures S3−S7 for the other dumbbells.[10] Single wavelength rises and decays determined at 380, 505, and 575 nm are best fit as multiple exponentials (Table 2). Data is not available for the 380 nm decay of **4**−**7** obtained using System 2 or for the 505 nm rise of **3**−**8** because of the overlap of the 505 nm band with the 575 nm band which is decaying on the same time scale.

The emissive band at 380 nm and the absorption band at 575 nm formed during the laser pump pulse are similar to those of hairpin **8** and are assigned to $^1Sa^*$ stimulated emission and absorption, respectively.[11] The initial fast 4−9 ps decay of the 575 nm band is attributed to vibrational relaxation of a locally excited $^1Sa^*$.[13] The 20−30 ps decay of the 385 nm band of **1**−**3** and the second 575 nm decay components of **1**−**8** (30−60 ps) are assigned to hole injection, which results in the formation of the bridge oxidized state $Sa^{-\bullet}-A_n^{+\bullet}-Sa$. The transient absorption spectrum of $Sa^{-\bullet}$ has a weak shoulder at 525 nm (absent in the transient spectrum of $^1Sa^*$) and an absorption maximum at 575 nm, whereas $A^{+\bullet}$ does not absorb in this wavelength region.[11]

Following the relatively fast events attributed to singlet relaxation and hole injection, the 380, 505, and 575 nm bands decay with one or more nanosecond decay components. Dumbbells **1**−**7** all have 575 nm band decays of about 1 ns, similar to the intermediate component of the fluorescence decays for **1**−**5** (Table 1). During this time period, the 505 nm band intensity continues to increase relative to that of the 575 nm band. The assignment of the 505 nm band to $Sa^{+\bullet}$ is supported by the similarity of the band maximum to those of structurally similar stilbene cation radicals[12,14] and by ZINDO calculations which show the absorption of $Sa^{+\bullet}$ to be blue-shifted from that of $Sa^{-\bullet}$ (λ_{max} = 460 and 520 nm, respectively).

Plots of the 505/575 nm band intensity ratios for **1**−**5** (Figure 3) display an initial fast rise to a value of about 0.38 with a

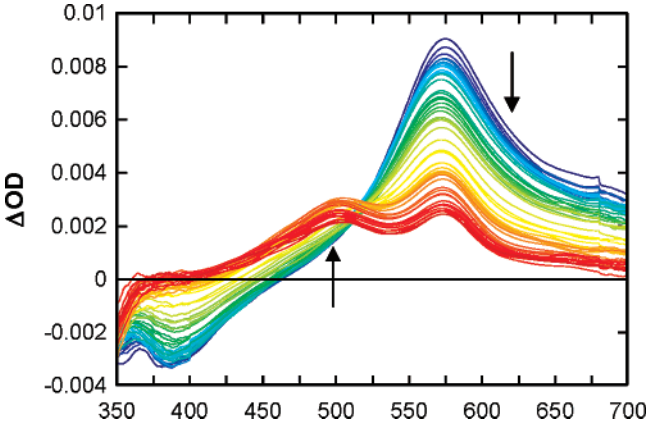

Figure 1. Transient absorption spectra for **1** obtained using System 1 at delay times of 0.5 ps to 1.8 ns following femtosecond laser excitation at 350 nm. Early spectra are shown in dark blue, and late spectra are shown in red. Arrows show the rise of the 505 nm band and decay of the 575 nm band.

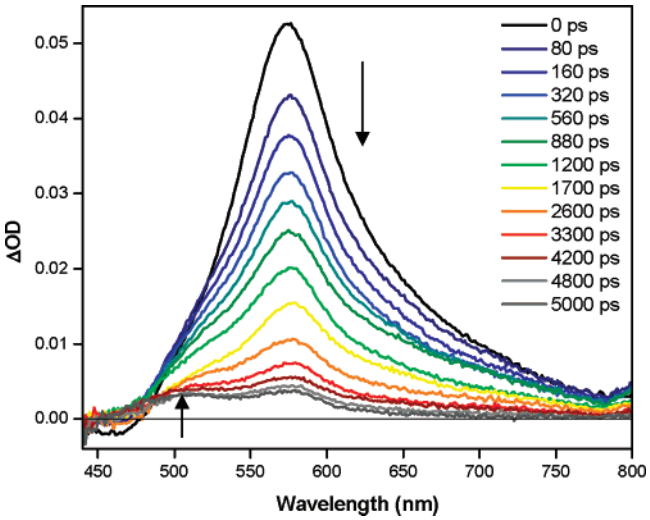

Figure 2. Transient absorption spectra of **5** obtained using System 2 at delay times of 0 ns (ΔOD/1.5) to 5 ns following femtosecond laser excitation at 350 nm. Arrows show the rise of the 505 nm band and decay of the 575 nm band.

time constant of about 40 ps assigned to hole injection and a slower rise assigned to formation of the $Sa^{-\bullet}-A_n-Sa^{+\bullet}$ charge-separated state (τ_1 and τ_2, Table 2). The band ratio rise times are thought to provide more accurate values for the hole injection rate and charge separation rate constant than the components of fluorescence decay because of the better time resolution of the transient absorption measurements. In the case of **1** and **2,** values of τ_1 and τ_2 are obtained from a double exponential fit to the experimental data (Figure 3) and a rising component in the 505 nm signal is observed that is similar to the value of τ_2 (Table 2). In the case of **3**−**6**, τ_2 is determined from the slopes of linear fits to the data in Figure 3. The use of initial rate kinetics may result in underestimation of the values of τ_2.[15] The absence of a second rising component for **7** and **8** is attributed to inefficient charge separation in **7** and the absence of a hole trap in **8**.

The decay of the 505 and 575 nm bands for **1**−**7** is incomplete on the nanosecond time scales of the femtosecond pump−probe experiments (2 ns for **1**−**3**, 6 ns for **3**−**7**, Figures 1−2 and S3−S7). Decay components larger than 2 ns are observed for the 505 nm decays of **1**−**3**, whereas a slow decay component could not be resolved for the weaker 505 nm transients from **4** and **5**. Nanosecond transient decays for **3**−**5** were acquired using a Nd:YAG laser system having a 6 ns pulse width for 355 nm excitation and a pulsed xenon arc lamp for detection with an instrument response time of about 7 ns.[16] Single wavelength 505 and 575 nm decays for **3**−**5** have decay times of about 7 ns, similar to the instrument response time.

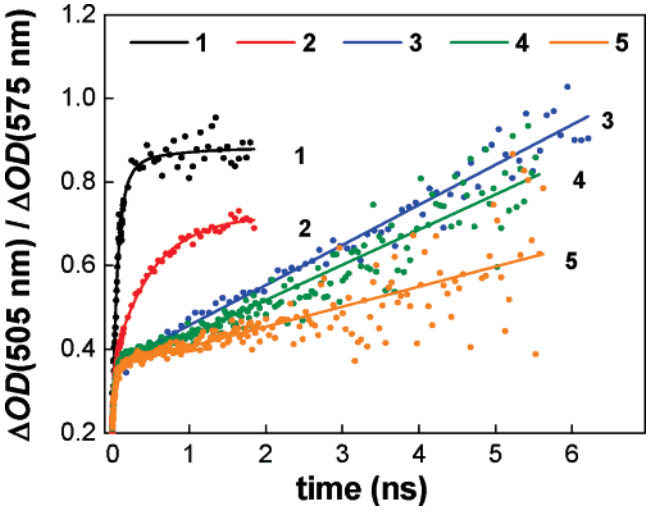

Figure 3. Time-dependent 505/575 band intensity ratio for **1**−**5**. The curved lines for **1**−**2** are double exponential fits of the data. The straight lines for **3**−**5** are linear fits of the data for times longer than 240 ps.

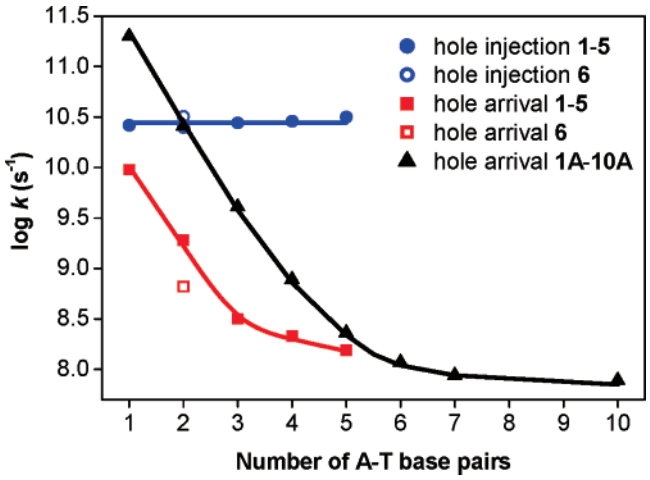

Figure 4. Rate constant for hole injection for $Sa-A_n-Sa$ dumbbells **1**−**6** and for hole arrival for dumbbells **1**−**6** and hairpins **1A**−**10A** (Chart 1).

Discussion

We have previously reported the synthesis and structural characterization of synthetic capped hairpin and dumbbell DNA conjugates having stilbenediamide (Sa) chromophores separated by a variable number of A−T base pairs.[8] The A-tract base-pair domains adopt B-DNA geometries and serve as helical scaffolds which define both the distance and the dihedral angle between the stilbene chromophores.[7] The stable well-defined B-DNA structures of the Sa/Sa dumbbells **1**−**7** make them well-suited for investigations of electronic interactions in the ground and excited electronic states.

Exciton coupling between Sa chromophores in **1**−**5** has little effect on the appearance of their UV and fluorescence spectra (Figures S1, S2). Only monomer fluorescence is observed, in accord with the absence of spatial overlap between the Sa chromophores.[17] The fluorescence quantum yields of **1**−**5** (Table 1) are all similar to that of hairpin **8**, which possesses a single

TABLE 2: Femtosecond Pump−Probe Transient Data for Dumbbells 1−7 and Hairpin 8[a]

	380 nm[b]	505 nm[c]	575 nm[d]				505/ 575 nm[e]	
conjugate	τ_1, ps[f]	τ_1, ps[g]	τ_1, ps[h]	τ_2, ps[f]	$\geq \tau_3$, ns[i]	τ_4, ns[i]	$\geq \tau_1$, ps[f]	τ_2, ns[g]
1	19	54	3.6 (26)	31 (44)	≥1 (30)		38	0.11
2	27	630	5.1 (20)	35 (42)	≥1 (38)		40	0.53
3	35		4.7 (15)	34 (35)	≥1 (50)	6.4	36	3.2[j]
4			9.1 (45)	62 (25)	1.1 (30)	7.1	35	4.8
5			8.7 (47)	61 (26)	1.1 (27)	6.3	32	6.6
6				84 (51)	1.1 (49)		31	1.7
7				59 (92)	1.4 (8)		∼40	
8[k]	23		8.9 (21)	43 (26)	≥ 1 (53)		39[l]	

[a] Data in aqueous solution (standard buffer) obtained using 350 nm excitation. [b] Single exponential fits to the 380 nm decay of stimulated emission; longer-lived components cannot be fit well to a second exponential. Data not available for **4**−**7** (see text). [c] Single exponential fits to the 505 nm rise (rising components not observed for **3**−**8**); additional long-lived components for **1**−**3** have estimated decay times of 4 ± 2 ns. [d] τ_1-τ_3 obtained from triple exponential fits to the 575 nm decay of the femtosecond pump−probe experiments (relative amplitudes in parentheses). A component having $\tau > 1$ ns is also observed but not fit. τ_4 is obtained from single exponential fits of the nanosecond pump−probe experiments. [e] Rise times for the 505/575 nm band intensity ratio; only one rising component was observed for **7** and **8**. [f] Component attributed to hole injection to the bridge. [g] Component attributed to hole arrival to Sa. [h] Component attributed to singlet relaxation. [i] Components attributed to charge return from $Sa^{-\bullet}-A_n^{\bullet+}-Sa$ and $Sa^{-\bullet}-A_n-Sa^{+\bullet}$. [j] Average of rise time obtained using laser Systems 1 and 2. [k] Data from ref 11. [l] Rising component of the 525/575 nm band ratio.

Sa chromophore (Chart 1), creating the erroneous impression that the two Sa chromophores do not interact in the excited state. The fluorescence decay times and amplitudes for **1**−**5** obtained from tri-exponential fitting are also similar, but differ from those for **8** (Table 1). This behavior is in marked contrast to that of the Sa−A_n−Sd capped hairpins (***n*A**, Chart 1) or Sa−A_n−G hairpins in which the fluorescence of ^{1}Sa* is substantially quenched at short distances and increases in intensity and lifetime as the length of the bridging A-tract increases. Fluorescence quenching in the Sa−A_n−G and Sa−A_n−Sd capped hairpins occurs via photoinduced charge separation leading to the formation of $Sa^{-\bullet}-A_n-G^{+\bullet}$ and $Sa^{-\bullet}-A_n-Sd^{+\bullet}$, which decay via charge recombination to form the ground state rather than via charge return to regenerate the locally excited Sa singlet state.[11,12,18]

Unlike the fluorescence properties of **1**−**7** (which provide no indication of interaction between the two Sa chromophores), the femtosecond transient absorption spectra of **1**−**7** (Figures 1, S3−S7) display changes in band shape indicative of the conversion of a locally excited ^{1}Sa* state to the $Sa^{-\bullet}-A_n-Sa^{+\bullet}$ charge-separated state. The assignment of the 575 and 505 nm bands to $Sa^{-\bullet}$ and $Sa^{+\bullet}$, respectively, is presented in the Results Section. Analysis of the results of transient absorption and fluorescence measurements supports the multistep mechanism for charge separation and charge return outlined in Scheme 1. According to this mechanism, charge separation occurs via a multistep process consisting of hole injection, hole transport against a Coulomb energy gradient, and hole trapping.[19] Charge recombination occurs by the reverse of this process—hole detrapping and hole return leading to ^{1}Sa* delayed fluorescence. Details of the hole injection, charge separation, and charge recombination processes are discussed in the following sections.

Hole Injection. The initial 40 ps rise in the 505/575 nm band intensity ratios of the transient absorption spectra of **1**−**7** (Figures 1−2 and S3−S7) is attributed to hole injection with formation of $Sa^{-\bullet}-A_n^{+\bullet}-Sa$ (Scheme 1). The 40 ps rise results from a combination of rate constants since hole injection is a reversible process, but it provides an approximate value for the hole injection rate constant ($k_i = \tau_1^{-1}$, Table 2).[11] Values of k_i for **1**−**7** are independent of the length of the base-pair domain (Figure 4) and are similar to the values reported for hairpin **8** and for donor-bridge acceptor Sa−A_n−Sd systems (Chart 1, ***n*A**) in which $n \geq 3$.[11,12] In the case of the Sa−A_n−Sd system in which $n = 1$ (**1A**), hole injection is slower than a single-step superexchange electron transfer that leads directly to the charge-separated state, whereas the hole injection process is the initial step in the charge separation process for **1**−**7** even at short distances (Figure 4).

The occurrence of superexchange electron transfer for short Sa−A_n−Sd capped hairpins but not for Sa−A_n−Sa dumbbells is consistent with the larger driving force for charge separation in the former system. The free energy change can be estimated using Weller's equation ($\Delta G_{et} = -E_s - E_{rdn} + E_{ox} - 0.1$ eV, where the constant term is the Coulomb attraction in water).[20] A value of $\Delta G_{et} = -0.52$ eV was reported for the Sa−A_n−Sd system,[11] whereas a value of $\Delta G_{et} = +0.15$ eV is obtained for the Sa−A_n−Sa system from the Sa singlet energy (3.35 eV) and peak potentials for its irreversible reduction and oxidation (−1.86 and 1.74 V, respectively, in DMF vs SCE). Stabilization of $Sa^{+\bullet}$ by π-stacking with the adjacent A−T base pair[21] or solvation by water may lower this value, rendering symmetry breaking approximately isoergonic.

The observation of similar k_i values for **1**−**7** indicates that the rate constant for hole injection is not strongly dependent upon the length or sequence of the adjacent A-tract. This suggests that the hole is initially localized on the adenine adjacent to the reduced Sa in what can be viewed as a contact ion pair, rather than being delocalized over two or more adjacent adenines in the A-tract.

Hole Transport and Trapping. The second rising component obtained from fitting the rise of the 505/575 nm band intensity ratio (Figure 3) is attributed to arrival of the hole at the Sa distal to the point of hole injection, resulting in the formation of $Sa^{-\bullet}-A_n-Sa^{+\bullet}$ (Scheme 1). The hole arrival time (τ_2, Table 2) is a complex function of the rate constants for reversible injection (k_i, k_{-i}), hole transport through the A-tract (k_{hop}, k_{-hop}), and hole trapping (k_t). In the case of **1** and **2,** the 505/575 nm band intensity ratio can be fit as the sum of two exponentials; however, for **3**−**5** an approximately linear increase in the band intensity ratio is observed between 0.2 and 6 ns (Figure 3). An initial slope method was thus used to obtain the values of τ_2.[12] The values of τ_2 provide approximate values for the rate constant for hole arrival k_a ($k_a \sim \tau_2^{-1}$) which decreases as the length of the A-tract increases (Figure 4). In the case of **1**, no hole transport is necessary and thus the value of k_a provides an upper limit of about 10^{10} s^{-1} for k_t. Since the hole arrival times for **2**−**5** are slower than 100 ps, the decrease in k_a is

attributed to an increase in the A-tract hole-transport time as the A-tract becomes longer.

The hole arrival times for Sa−A_n−Sd capped hairpin systems also increase with increasing n (Figure 4).[11,12] However, the values of k_a are significantly faster for Sa−A_n−Sd than for Sa−A_n−Sa systems, especially at shorter distances, indicative of faster hole trapping by the deeper Sd hole trap. The values of k_a for Sa−A_n−Sa and Sa−A_n−Sd systems converge for longer A-tracts, as expected for rate-limiting hole transport in both systems. Thus hole arrival times for systems having long A-tracts appear to be independent of the depth of the hole trap.

The efficiency of charge separation for the dumbbell systems has not been directly measured but decreases significantly for the series **1**−**5**, based on the relative intensities of the 505 nm bands in the transient spectra (Figures 1−2 and S3−S7). A similar decrease in the efficiency of charge separation has been observed for Sa−A_n−Sd systems.[12] A plausible explanation for this distance dependence is Coulomb attraction between $Sa^{-\bullet}$ and holes residing on A in the bridge.[19] The Coulomb stabilization is largest for the contact ion pair $Sa^{-\bullet}-A^{+\bullet}$ and decreases asymptotically as the distance between charges increases. Increasing energy of the bridge-oxidized state with increasing distance between $Sa^{-\bullet}$ and $A^{+\bullet}$ should result in decreases in both the rate constant and quantum yield for hole arrival, which become smaller as the energy levels converge at longer distances (Scheme 1).

The k_a value for dumbbell **6** which has an AT bridge sequence is smaller than that for **2** (Figure S8) as is its charge separation efficiency. In the case of **7**, which has an ATA bridge sequence, the 505 nm band intensity is too weak to permit reliable measurement of k_a. Thus, both the rate constant for hole arrival and the efficiency of charge separation are smaller for alternating AT than for A-tract bridges. This observation is consistent with other reports of AT vs A_n hole transport[22] and with our recent study of the dynamics and efficiency of hole transport in Sa−$(TA)_n$−Sd systems.[23]

Charge Return. The observation of similar fluorescence quantum yields and delayed fluorescence lifetimes for **1**−**5** (Table 1) requires that charge return from the $Sa^{-\bullet}-A_n^{+\bullet}-Sa$ and $Sa^{-\bullet}-A_n-Sa^{+\bullet}$ charge-separated states results in repopulation of locally excited $^1Sa^*$ (Scheme 1). There is ample precedent for delayed fluorescence resulting from the equilibrium between locally excited and charge-transfer excited states.[3,5] We have previously observed delayed fluorescence for hairpin **8** and Sa−A_n−Sd capped hairpins ($n \geq 2$), and attributed it to charge return from the $Sa^{-\bullet}-A_n^{+\bullet}-Sd$ states.[11] The approximately 1 ns components of fluorescence decay (Table 1) and of the 575 nm transient decay of $Sa^{-\bullet}$ (Table 2) for **1**−**5** are similar to those measured for Sa−A_n−Sd systems, and they are assigned to charge return from bridge-oxidized $Sa^{-\bullet}-A_n^{+}-Sa$ states.

The transient spectra of the $Sa^{-\bullet}-A_n-Sa^{+\bullet}$ charge-separated states of **1**−**5** are persistent on the 2 and 6 ns time scales of the femtosecond transient absorption measurements, in accord with the observation of a long-lived component of fluorescence decay (Table 1). Fits of the 575 nm decays for **1**−**3** have decay components ≥1 ns (Table 2); however, the long-lived transients for **4** and **5** are too weak to permit fitting of the femtosecond transient data (Figures 2 and S5). Nanosecond transient absorption decays for **3**−**5** are similar to the 7 ns instrument response time. On the basis of these observations and on the measurement of identical fluorescence quantum yields for **1**−**5**, we conclude that charge recombination of $Sa^{-\bullet}-A_n-Sa^{+\bullet}$ occurs on the 2−10 ns time scale and results predominantly in return to the fluorescent locally excited state $^1Sa^*-A_n-Sa$. The absence of a pronounced distance dependence is indicative of a mechanism in which hole detrapping is rate-determining and charge recombination may be faster than charge separation for the longer dumbbells **3**−**5**. Following detrapping, charge recombination of the $Sa^{\bullet-}-A_n^{+\bullet}-Sa$ charge-separated states in a Coulomb gradient should be faster than charge separation. The ratio of time constants for hole trapping in **1** (ca. 100 ps) and detrapping in **3**−**5** (ca. 5 ns) provides an estimated value of about 0.05 eV for the free energy of hole trapping.

Charge recombination via bridge-mediated thermal hole detrapping in DNA has not been previously observed, however hole detrapping is an essential step in the transport of holes between guanine-containing trapping sites in DNA.[24] Hole detrapping does not compete with single step superexchange as the mechanism for charge recombination in $Sa^{-\bullet}$-A_n-$Sd^{+\bullet}$ and other systems having deep hole traps.[11] Charge recombination is strongly distance-dependent in these systems, and the charge-separated states have long lifetimes (ca. 30 μs for $Sa^{-\bullet}$-A_n-$Sd^{+\bullet}$ when $n = 5$).[11] Evidently hole detrapping does not compete effectively with superexchange in the case of Sd, G, and other relatively deep hole traps such as phenothiazine.[25,26] The guanine hole trap is estimated to lie 0.2−0.4 eV below the A-tract[25] and the Sd hole trap is even deeper (ca. 0.5 eV).[11]

Conclusion

In summary, excited-state symmetry breaking in Sa−A_n−Sa dumbbells occurs via a bridge-mediated charge separation process consisting of hole injection, hole transport, and hole trapping (Scheme 1). To our knowledge, this is the first example of symmetry breaking in an A−B−A system via a bridge-mediated hole-hopping mechanism. The occurrence of symmetry breaking in Sa−A_n−Sa dumbbells is a consequence of both the unique ability of A-tract DNA to mediate hole transport and the highly polar aqueous solvent. Hole transport is the rate-determining step for symmetry breaking in dumbbells possessing more than one A−T base pair. It is interesting to note that charge separation occurs in preference to delocalization of electronic excitation, even though the energetics of charge separation are marginally favorable.

Charge recombination of the $Sa^{-\bullet}-A_n-Sa^{+\bullet}$ charge-separated state occurs by the reverse of the charge separation process: hole detrapping followed by charge return to regenerate the $^1Sa^*-A_n-Sa$ locally excited state. Charge recombination via a multistep hole-transport mechanism has not been previously observed in a DNA-based system. However, we have recently observed relatively fast ($\tau \sim 100$ ps) and weakly distance-dependent charge recombination via hole detrapping in a tertiary arylurea donor−bridge−acceptor (D−B−A) system.[27]

The kinetics of hole arrival and charge return for Sa−A_n−Sa systems (Figure 4) serve to further elucidate the overall dynamics of charge separation and recombination processes in DNA. Our kinetic results would appear to be compatible with either a hole-hopping mechanism in which the hole is largely localized on a single adenine[28] or a hole-transport mechanism in which the hole is delocalized over several adjacent adenines.[29] The complex kinetics of the symmetry-breaking charge-separation and charge-recombination processes makes it impossible to assign rate constants to the individual kinetic steps in Scheme 1. These results underscore the hazards of using a single steady-state measurement such as the relative fluorescence quantum yield or strand cleavage efficiency as a proxy for hole-transport dynamics and efficiency. In the case of the Sa−A_n−Sa

dumbbells, there is no fluorescence quenching in spite of the occurrence of rapid and efficient hole injection.

Experimental Section

Dumbbells **1**−**7** were synthesized using the method previously reported for the synthesis of **1**−**5**.[8] They were purified by reverse-phase HPLC and characterized by their UV, fluorescence, and MALDI-TOF mass spectra. All solutions were prepared in 10 mM sodium phosphate buffer (pH 7.2) containing 0.1 M NaCl. Hairpin concentrations were adjusted to provide absorbances at 355 nm of about 0.2 for fluorescence measurements (1 cm path length) and 0.3 for transient absorption measurements (1 or 2 mm path length). Fluorescence quantum yields were obtained using quinine sulfate as an external reference standard.[30] Measurements of fluorescence decays, nanosecond transient absorption decays, and femtosecond broad−band pump−probe spectra were performed as previously described.[11,12,16]

Acknowledgment. This research is supported by the Office of Basic Energy Sciences, U.S. Department of Energy under Contract DE-FG02-96ER14604 (FDL) and DE-FG02-99ER14999 (MRW), and by grants from the Volkswagen Foundation (TF) and the Kresge Foundation (VS).

Supporting Information Available: UV absorption (Figure S1) and fluorescence spectra (Figure S2), transient absorption spectra for **2**−**4** and **6**−**7** (Figures S3−S7), and comparison of the time-dependent band intensity ratios for **2** and **6** (Figure S8). This material is available free of charge via the Internet at http://pubs.acs.org.

References and Notes

(1) Michl, J.; Bonacic-Koutecky, V. *Electronic Aspects of Organic Photochemistry*; Wiley-Interscience: New York, 1990.

(2) Schneider, F.; Lippert, E. *Ber. Bunsen-Ges. Phys. Chem.* **1968**, *72*, 1155−1160. Piet, J. J.; Schuddeboom, W.; Wegewijs, B. R.; Grozema, F. C.; Warman, J. M. *J. Am. Chem. Soc.* **2001**, *123*, 5337−5347.

(3) Yao, H.; Okada, T.; Mataga, N. *J. Phys. Chem.* **1989**, *93*, 7388−7394.

(4) Giaimo, J. M.; Gusev, A. V.; Wasielewski, M. R. *J. Am. Chem. Soc.* **2002**, *124*, 8530−8531.

(5) Holman, M. W.; Liu, R.; Zang, L.; Yan, P.; DiBenedetto, S. A.; Bowers, R. D.; Adams, D. M. *J. Am. Chem. Soc.* **2004**, *126*, 16126−16133.

(6) Holman, M. W.; Yan, P.; Adams, D. M.; Westenhoff, S.; Silva, C. *J. Phys. Chem. A* **2005**, *109*, 8548−8552.

(7) Lewis, F. D.; Zhang, L.; Liu, X.; Zuo, X.; Tiede, D. M.; Long, H.; Schatz, G. S. *J. Am. Chem. Soc.* **2005**, *127*, 14445−14453.

(8) Zhang, L.; Long, H.; Schatz, G. C.; Lewis, F. D. *Org. Biomol. Chem.* **2007**, *5*, 450−456.

(9) Lewis, F. D.; Wu, T.; Burch, E. L.; Bassani, D. M.; Yang, J.-S.; Schneider, S.; Jäger, W.; Letsinger, R. L. *J. Am. Chem. Soc.* **1995**, *117*, 8785−92. Anger, I.; Sandros, K.; Sundahl, M.; Wennerstroem, O. *J. Phys. Chem.* **1993**, *97*, 1920−1923.

(10) Information provided as Supporting Information.

(11) Lewis, F. D.; Zhu, H.; Daublain, P.; Fiebig, T.; Raytchev, M.; Wang, Q.; Shafirovich, V. *J. Am. Chem. Soc.* **2006**, *128*, 791−800.

(12) Lewis, F. D.; Zhu, H.; Daublain, P.; Cohen, B.; Wasielewski, M. R. *Angew. Chem., Int. Ed.* **2006**, *45*, 7982−7985.

(13) Lewis, F. D.; Wu, T.; Liu, X.; Letsinger, R. L.; Greenfield, S. R.; Miller, S. E.; Wasielewski, M. R. *J. Am. Chem. Soc.* **2000**, *122*, 2889−2902.

(14) Samori, S.; Hara, M.; Tojo, S.; Fujitsuka, M.; Majima, T. *J. Photochem. Photobiol. A* **2006**, *179*, 115−124.

(15) For a discussion of initial-rate kinetics, see: Anslyn, E. V.; Dougherty, D. A. *Modern Physical Organic Chemistry*; University Science Books: 2004.

(16) Shafirovich, V.; Dourandin, A.; Huang, W.; Luneva, N. P.; Geacintov, N. E. *J. Phys. Chem. B* **1999**, *103*, 10924−10933.

(17) Winnik, F. M. *Chem. Rev.* **1993**, *93*, 587−614.

(18) Lewis, F. D.; Wu, Y.; Zhang, L.; Zuo, X.; Hayes, R. T.; Wasielewski, M. R. *J. Am. Chem. Soc.* **2004**, *126*, 8206−8215.

(19) Grozema, F. C.; Tonzani, S.; Berlin, Y. A.; Schatz, G. C.; Siebbeles, L. D. A.; Ratner, M. A. *J. Am. Chem. Soc.*, accepted for publication.

(20) Weller, A. *Zeit. Phys. Chem.* **1982**, *133*, 93−98.

(21) Voityuk, A. A.; Jortner, J.; Bixon, M.; Rösch, N. *Chem. Phys. Lett.* **2000**, *324*, 430−434. Fukuzumi, S.; Nishimine, M.; Ohkubo, K.; Tkachenko, N. V.; Lemmetyinen, H. *J. Phys. Chem. B* **2003**, *107*, 12511−12518.

(22) Nakatani, K.; Dohno, C.; Saito, I. *J. Am. Chem. Soc.* **1999**, *121*, 10854−10855.

(23) Lewis, F. D.; Daublain, P.; Cohen, B.; Vura-Weis, J.; Shafirovich, V.; Wasielewski, M. R. *J. Am. Chem. Soc.* **2007**, *129*, 15130−15131.

(24) *Long-Range Charge Transfer in DNA*; Schuster, G. B., Ed.; Springer-Verlag: Berlin, 2004.

(25) Takada, T.; Kawai, K.; Fujitsuka, M.; Majima, T. *Chem. Eur. J.* **2005**, *11*, 3835−3842.

(26) Takada, T.; Kawai, K.; Fujitsuka, M.; Majima, T. *J. Am. Chem. Soc.* **2006**, *128*, 11012−11013.

(27) Zeidan, T. A.; Wang, Q.; Fiebig, T.; Lewis, F. D. *J. Am. Chem. Soc.* **2007**, *129*, 9848−9849.

(28) Jortner, J.; Bixon, M.; Langenbacher, T.; Michel-Beyerle, M. E. *Proc. Natl. Acad. Sci. U.S.A.* **1998**, *95*, 12759−12765. Berlin, Y. A.; Burin, A. L.; Ratner, M. A. *J. Am. Chem. Soc.* **2001**, *123*, 260−268.

(29) Schuster, G. B. *Acc. Chem. Res.* **2000**, *33*, 253−260. Conwell, E. M.; Rakhmanova, S. V. *Proc. Natl. Acad. Sci. U.S.A.* **2000**, *97*, 4556−4560.

(30) Kuhn, H. J. *Pure Appl. Chem.* **2004**, *76*, 2105−2146.